The importance of fuel variability on the performance of solid oxide cells operating on H_2/CO_2 mixtures from biohydrogen processes

Authors: Christian J. Laycock*, Kleitos Panagi, James P. Reed and Alan J. Guwy

Sustainable Environment Research Centre, University of South Wales, Upper Glyntaff, Pontypridd, CF37 4BD, United Kingdom

*Corresponding author.

Email: christian.laycock@southwales.ac.uk

Tel: +44 (0)1443 654596

Abstract

Biologically produced mixtures of H_2 and CO_2 (biohydrogen) from processes such as dark fermentation or photo-fermentation are versatile feedstocks which can potentially be utilised in solid oxide cell (SOC) devices. In this work, solid oxide electrolysis of biohydrogen has been investigated for the first time and is compared directly with fuel cell mode utilisation. The performance and fuel processing of SOCs utilising biohydrogen have been characterised in greater detail than has been achieved previously through the use of experiments which combine electrochemical techniques with quadrupole mass spectrometry (QMS). The effects of fuel variability on SOC overpotentials and outputs have been established and it is shown that cell performance is not significantly affected provided the fuel composition stays within 40-60 vol% H_2. QMS measurements indicate H_2O and CO production takes place *in-situ* via the reverse water-gas shift (RWGS) reaction. Electrical power production in fuel cell mode is predominantly through H_2 oxidation, whilst CO is converted in the WGS reaction to regenerate CO_2 but does not contribute to electrical power production. In electrolysis mode, CO is produced simultaneously through electrochemical CO_2 reduction and the RWGS reaction; H_2O is electrochemically reduced to regenerate H_2.

Keywords

Solid oxide fuel cell; solid oxide electrolysis; biohydrogen; fuel variability; fuel processing; reverse water gas shift.

1. Introduction

Solid Oxide Cells (SOCs) are high temperature electrochemical energy conversion devices that are made with a ceramic electrolyte material [1-5]. They are highly efficient, operate silently and can be sized from 1 kW_e to 1 MW_e upwards due to their modular and scalable design. When operating in fuel cell mode, SOCs (Solid Oxide Fuel Cells (SOFCs)) convert the chemical energy in fuels directly into electrical and heat energy and produce fewer emissions compared with conventional combustion systems. The heat energy produced potentially enables deployment in micro Combined Heat and Power (μCHP) applications. In electrolysis mode, SOCs (Solid Oxide Electrolysis Cells (SOECs)) consume electrical power and heat energy to convert gaseous oxidants into useful fuels and chemicals [6-15]. Unlike low temperature electrolysers, they can convert mixtures of H_2O and CO_2 into synthesis gas (H_2 + CO). The high operating temperature and oxygen ion charge transport of SOCs enables operation on hydrogen-, carbon- and nitrogen-based feedstocks, whereas many other fuel cell and electrolyser technologies are limited to pure H_2 or H_2O only.

This fuel flexibility gives SOCs the capability to utilise a wide range of complex feedstocks including renewable fuels such as biogas (CH_4/CO_2) [16-23] and biohydrogen (H_2/CO_2) [24-29], in addition to gas mixtures from gasification processes [30-33] and industrial waste gases [34-37]. However, the compositions of these gaseous feedstocks are inherently variable due to the processes by which they are produced [24,38-44]. Fuel variability has been shown to affect the stability, efficiency and durability of SOC devices and therefore alleviating the effects caused by variation in fuel composition is key to the efficient utilisation of renewable and industrial waste feedstocks in SOC devices [28,45-48].

In this work, the performance and fuel variability effects of a commercially available electrolyte-supported cell (ESC) running on simulated biohydrogen mixtures have been investigated. A brief literature review provides an overview of previous work into biohydrogen utilisation in SOCs, which has focussed on fuel cell mode characterisation using

computational and electrochemical techniques. Experimental investigations that combine electrochemical techniques with quadrupole mass spectrometry (QMS) are then reported which characterise the performance and fuel processing of biohydrogen utilisation in SOCs in greater detail than has been achieved previously. In addition, solid oxide electrolysis of biohydrogen has been investigated for the first time and is compared directly with biohydrogen utilisation in fuel cell mode. The effects of fuel variability on SOC overpotentials and outputs are also established.

2. Utilisation of Biohydrogen in SOC Devices

There has been a significant amount of previous research into the utilisation of methane-rich biogas produced by anaerobic digestion (AD) in SOFCs [16-23]. Methane-rich biogas mixtures are variable and have a typical CH_4/CO_2 composition of 60/40 vol%. They also contain variable levels of trace components such as hydrogen sulfide, ammonia, siloxanes, and tars [38-40]. Amongst other things, poor resistance towards carbon deposition (caused by excessive methane decomposition) and poisoning by fuel impurities such as hydrogen sulfide make the utilisation of biogas in SOCs very challenging [49-54].

Mixtures of H_2 and CO_2 can produced from numerous processes including dark fermentation, photo-fermentation, indirect biophotolysis and bioelectrochemical techniques [55-58]. H_2/CO_2 mixtures produced from these types of processes are widely known as ‘biohydrogen’ and typically have a 50/50 vol% H_2/CO_2 content (see Table 1). Like methane-rich biogas mixtures, they are variable and contain trace levels of sulfur-, nitrogen-, and carbon-based contaminants [24,27]. Crucially, they avoid the need to handle methane, which is a very potent greenhouse gas.

Table 1. Typical composition of gases from biohydrogen production processes [24].

Component	Content
Hydrogen	35-50 vol%
Carbon dioxide	50-55 vol%
Nitrogen	3-8 vol%
Oxygen	1-4 vol%
Carbon monoxide	< 0.001 vol%
Methane	< 0.01 vol%
Sulfur-containing compounds	< 200 ppm
Other impurities	< 2 vol%

Biohydrogen mixtures can potentially be utilised in various technologies including combustion devices and fuel cell technology [24-29,59-62]. Combustion engines and low temperature fuel cells require prior removal of CO_2 due to the very strict fuel composition requirements of these devices. Gas upgrading has been well studied for biogas to biomethane processes [61-64] and a comparison of established gas upgrading technologies is shown in Table 2. Each technology requires electrical energy and in some cases heat energy, whilst most also have a consumables demand and do not operate effectively under partial load. In addition, the use of a gas upgrading technology represents a capital and operational cost to the consumer. Furthermore, there is an inevitable loss of fuel, which decreases the net energy gain and causes fugitive fuel emissions.

Table 2. Comparison of biogas upgrading technologies. Information and values applicable for production of biomethane from biogas [61-64].

Parameter	Water Scrubbing	Organic Physical Scrubbing	Amine Scrubbing	Pressure Swing Absorption	Membrane Separation
Electrical Energy Demand / kWh m^{-3}	0.40 – 0.50	0.45 – 0.70	0.25 – 0.35	0.40 – 0.50	0.25 – 0.45
Operating Temperature / °C	-	70 – 80	120 – 160	-	-
Consumables Demand	Antifouling and drying agents	Organic solvents	Amine-based solvents	Activated carbon	-
Partial Load Range	50 – 100 %	50 – 100 %	50 – 100 %	85 – 100 %	50 – 100 %
Typical Capital Costs / € $(m^3\ h^{-1})^{-1}$	3.5 – 10.0	3.5 – 9.5	3.5 – 9.5	3.7 – 10.0	3.5 – 7.6
Typical Operational Costs / € m^{-3}	0.09 – 0.14	0.09 – 0.14	0.11 – 0.14	0.09 – 0.13	0.07 – 0.16
Methane Recovery	98 %	96 %	> 99 %	98 %	80 – 99.5 %

Utilisation of biohydrogen in SOC technology removes the need to upgrade the fuel mixture because SOC devices are fuel flexible and are not affected by the presence of CO_2. Desulfurisation of biohydrogen would still be necessary but would not require an energy intensive or complex gas upgrading system. In fact, the significant presence of H_2 would likely increase the sulfur tolerance of SOCs in comparison with operation on a carbon-based fuel such as natural gas or biogas [24-25,65]. The absence of methane in biohydrogen has been shown to make SOCs less prone towards carbon deposition, which is a significant problem for operation on methane-based fuel mixtures [16-24]. Utilisation of biohydrogen in SOCs has been demonstrated in fuel cell mode with comparable performance to that observed when operating on pure H_2 [29]. Biohydrogen is more versatile than biogas and can also potentially be very efficiently electrolysed in SOCs to yield useful mixtures of synthesis gas (H_2 + CO). Conversion of biohydrogen in a reversible SOC device therefore also gives energy production and storage flexibility, since electrical power or synthesis gas can be produced as required using a single SOC device with efficiencies as high as 70%,

reducing investment costs and payback times. However, significant technological development is required in order to reduce the capital costs of SOC devices [6-15].

Previous work into the utilisation of biohydrogen in SOC devices has focussed on fuel cell mode operation to yield electrical power and heat [24-29]. Leone *et al*. [24-25] have shown that conversion of biohydrogen is closely related to the reverse water-gas shift (RWGS) reaction:

$$H_2 + CO_2 \rightleftharpoons H_2O + CO \quad (1)$$

A computational study by Razbani *et al*. [26] illustrated the importance of the RWGS reaction to the performance and cooling requirements of SOCs running on biohydrogen. The RWGS reaction is kinetically fast and thermodynamically favourable over nickel catalysts at SOC operating temperatures [66-69]. It causes the presence of H_2 to decrease and CO to increase, and therefore has a negative effect on the open circuit potential (OCP) of SOCs. The RWGS reaction is mildly endothermic (ΔH = +41 kJ mol^{-1}) and therefore reduces stack cooling requirements in comparison with pure H_2 or H_2/N_2 mixtures; however, stack cooling requirements are increased in comparison with biogas utilisation in SOCs, where fuel conversion proceeds simultaneously with the highly endothermic CO_2 (ΔH = +247 kJ mol^{-1}) or steam reforming (ΔH = +205 kJ mol^{-1}) reactions [15-23]. Nevertheless, the overall performance and durability of SOCs is better for biohydrogen due to the absence of methane, which causes significant problems relating to carbon deposition for SOCs running on biogas mixtures [27].

A separate study by Razbani *et al*. [28] investigated the effects of various SOC operating parameters on biohydrogen utilisation. It was shown that increasing the operating temperature increases the overall cell performance due to increased activation and ohmic efficiencies, as well as a shift in the RWGS equilibrium. In addition, investigations into fuel variability show that cell performance is generally increased with increasing H_2 content of the

fuel due to decreased activation losses, better heat distribution across the cell from the fuel cell reactions and the reduced cooling effects of the RWGS reaction at high temperatures.

Whilst previous studies have focussed on fuel cell mode characterisation of SOCs running on biohydrogen predominantly using computational and electrochemical techniques, the following experimental investigations characterise biohydrogen utilisation in SOCs using a combination of electrochemical techniques and QMS, which have enabled the performance and fuel processing to be investigated in significantly greater detail than has been achieved previously. In addition, solid oxide electrolysis of biohydrogen has been investigated for the first time and is compared directly with fuel cell mode performance and products. Finally, the effects of fuel variability on SOC performance and products have been established.

3. Materials and Methods

The electrochemical performance of the cell was investigated using potentiostatic measurements, current-voltage curves and electrochemical impedance spectroscopy. The fuel processing chemistry at the anode was investigated by continuous analysis of the output gas composition using QMS. The performance, fuel processing and products of the ESC were studied: (1) at the open circuit potential (OCP) in order to determine OCP losses; (2) when running on non-variable 50/50 vol% H_2/CO_2 mixtures in order to investigate fuel supply and operating voltage effects; and (3) when supplied with different H_2/CO_2 compositions in order to investigate the effects of fuel variability.

3.1 Mounting and conditioning of the ESC

All measurements and testing were carried out at 800 °C using a commercially available electrolyte-supported Button Cell (FCM, NextCell-2.0, 213205) composed of a 150 µm thick scandium-stabilised zirconia electrolyte, a 50 µm NiO-GDC/NiO-YSZ anode and a 50 µm LSM/LSM-GDC cathode (where GDC is gadolinia-doped ceria). The diameter of the electrolyte was 20 mm and the diameter of both electrodes was 12.5 mm.

The cell was tested using a Fiaxell Open Flanges SOFC test set-up. Detailed information on the test set-up is available on the Fiaxell website [70]. The ESC was mounted within two spring-loaded flanges on the underside of the test set-up. The flanges were made with Inconel 600 and 601 and enabled feeding of air and fuel gases to the cell. A gas-tight seal preventing fuel and oxidant crossover was created by pressing the cell between two sheets of alumina felt within the flanges. Electrical current collection wires were also positioned within the alumina felt sheets. Gold wire mesh was used for current collection at the cathode and nickel foam was used for current collection at the anode. The temperature of the cell was measured using a type-K thermocouple, which was positioned above the cell on top of the alumina felt. The cell, wires, nickel foam and thermocouple were held in position during mounting using silica-free tape and adhesive. The flanges were then spring loaded, completing the cell mounting procedure.

Once mounted, the underside of the test set-up was placed within a chamber furnace which was used to heat the cell to the required temperature. The current collection and voltage sensing wires were connected to a potentiostat (Ivium Technologies IviumStat), enabling electrochemical measurements to be carried out. Gas delivery and recovery connections were made using stainless steel Swagelok fittings. Air (Air Liquide, 99.99%) was supplied to the cathode using a rotameter. Fuel gases were supplied to the anode using a Bronkhorst Flow-SMS digital mass flow controller system, which enabled the delivery of gaseous mixtures containing H_2 (Air Liquide, 99.999%), CO_2 (Air Liquide, 99.99%) and He (Air Liquide, 99.999%). Product gases from the anode were collected continuously and fed into a quadrupole mass spectrometer (Cyionics Ltd.) fitted with an IOTA residual gas analyser, enabling continuous measurement of the product gas composition.

The test set-up was initially heated at 120 °C h^{-1} up to 400 °C, followed by a second heating ramp of 200 °C h^{-1} up to 800 °C. During initial heating, air was supplied at 200 cm^3 min^{-1} to both the anode and cathode in order to burn off the tape and adhesive used during cell mounting. When the cell reached 800 °C, the spring-loaded pressure of the flanges was

checked and corrected as required. All measurements reported in this paper were collected at 800 °C.

After heating, the fuel delivery line and anode were purged with 30 cm^3 min^{-1} of helium for 30 minutes in order to displace air. 5 vol% H_2 was then added to the mixture in order to reduce the anode and nickel foam. Reduction of the anode was monitored by observing the OCP of the cell. When the OCP had stabilised, the H_2 content was increased to 10 vol% until the OCP had re-stabilised. This procedure was repeated until the gas stream consisted of 100 vol% H_2. The OCP observed under pure H_2 was 1.1090 V at 800 °C, indicating negligible gas crossover and current loss. Finally, a voltage of 0.8 V was applied to the cell for 24 hours in order to condition the electrolyte.

3.2 Electrochemical measurements

The electrochemical performance of the cell was studied in fuel cell mode and electrolysis mode. H_2/CO_2 gas mixtures containing 10 - 100 vol% H_2 (balanced with CO_2) were supplied to the cell as required. The fuel mixture was supplied at 30 cm^3 min^{-1}. The OCP or current output (as required) of the cell were then left to stabilise for 20 minutes before taking any measurements. For fuel cell mode measurements, 50 cm^3 min^{-1} of air was supplied to the cathode. No air was supplied when the cell was studied in electrolysis mode, leaving only static air present at the cathode.

Current-voltage (I-V) curves were measured over the range OCP - 0.1 V in fuel cell mode, and in electrolysis mode were measured in the range OCP - 1.9 V. All I-V curves were measured potentiostatically at a scan rate of 50 mV s^{-1}. Electrochemical impedance spectroscopy (EIS) measurements were taken potentiostatically over the frequency range 0.1 kHz - 100 MHz using a voltage amplitude of 10 mV. EIS measurements were carried out in fuel cell mode at 0.1 V below the OCP and in electrolysis mode at 0.1 V above the OCP.

3.3 Anode output gas analysis using quadrupole mass spectrometry

The composition of the output gases leaving the anode was measured using QMS. The spectrometer was primarily set to measure the intensities of m/z = 2 (H_2), 28 (CO), and 44 (CO_2). The sensitivity of the spectrometer towards each of the gases was measured and used for data correction, so that the data presented in this work represents the relative partial pressures of the output gases leaving the cell. Helium (m/z = 4) was used as the carrier gas. When taking QMS measurements, fuel gases were delivered at a rate of 8 cm^3 min^{-1} and were diluted in 22 cm^3 min^{-1} of helium to give a total gas flow rate to the cell of 30 cm^3 min^{-1}. It was necessary to remove H_2O present in the output gases using a silica gel desiccant in order to prevent flooding of the QMS capillary inlet line. The presence of H_2O in the output gases was therefore not measured.

The effect of fuel composition on the output gases leaving the anode was measured at the OCP, in fuel cell mode and electrolysis mode when running on H_2/CO_2 mixtures containing 25 - 100 vol% H_2 (balanced with CO_2) as required. The composition of the output gases leaving the anode were measured for approx. 20 minutes under each composition.

The performance of the cell running on a non-variable 50/50 vol% H_2/CO_2 mixture was investigated for the purposes of control measurements and to investigate the effects of operating voltage. These measurements were carried out over the voltage range OCP - 0.1 V (fuel cell mode) and OCP - 1.8 V (electrolysis mode). These measurements were collected potentiostatically by changing the electrical load in 0.1 V increments and measuring the composition of the output gases for approximately 15 minutes at each voltage. The current output of the cell was measured separately and correlated with the QMS data.

4. Results and Discussion

4.1 Effect of fuel variability on OCP

The effect of H_2/CO_2 composition on the OCP of the cell is shown in Fig. 1a alongside the theoretical Nernst potential which decreased linearly as the H_2/CO_2 composition was varied from 100/0 – 10/90 vol%. Under pure H_2, the experimentally measured OCP agreed closely with the Nernst potential, indicating the cell was well sealed with minimal gas crossover and current loss. Adding CO_2 to the fuel mixture immediately caused the OCP to deviate sharply away from the Nernst potential in a manner consistent with previously reported theoretical and experimental trends [24-29]. The OCP decreased non-linearly as the CO_2 content was increased to approx. 20 vol%. From 20-60 vol% CO_2, the OCP decreased almost linearly and in parallel with the Nernst potential before again decreasing non-linearly as the CO_2 content was increased above 60 vol%.

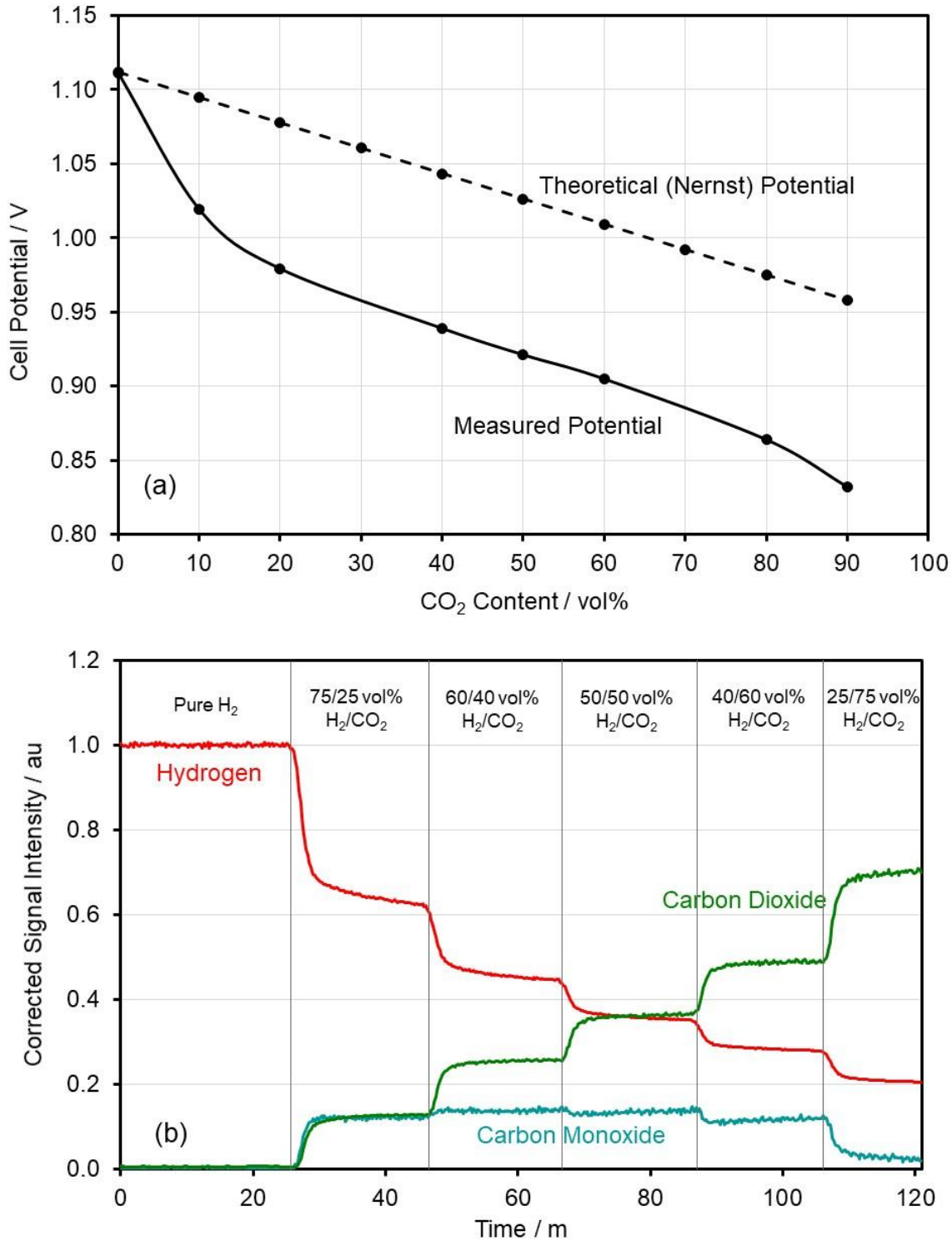

Fig. 1. The effect of H_2/CO_2 fuel composition on: (a) the OCP of the ESC, and (b) the composition of the output gases leaving the anode at OCP. The temperature of the ESC was 800 °C.

The deviation of the OCP away from the theoretical Nernst potential is explained by the presence of the RWGS reaction (1), which was observed by analysis of the product gases leaving the anode as shown in Fig. 1b. At 75/25 vol% H_2/CO_2, the levels of H_2 and CO_2

leaving the anode were less than 0.75 au and 0.25 au respectively, and CO was detected. The signal intensities of masses 15 and 31 were measured to check for the presence of CH_4 and CH_3OH respectively but none were found, suggesting the presence of other reactions such as methanation were not significant and implying the presence of the RWGS reaction.

Fig. 1b shows the presence of CO did not change significantly as the CO_2 content of the input gases was increased from 25 - 60 vol%, indicating the H_2/CO_2 composition did not have a significant effect on the equilibrium of the RWGS reaction over this range. This explains the linear decrease of OCP observed over this range in Fig. 1a; the equilibrium of the RWGS reaction was not changed and therefore the OCP varied linearly and in parallel with the theoretical Nernst potential due to a proportional dilution of the gases in CO_2. The sharp deviation of the OCP away from the Nernst potential at 0 - 25 vol% CO_2 was due to the equilibrium of the RWGS reaction, which was strongly influenced by the H_2/CO_2 composition over this range. Adding CO_2 did not therefore cause a simple dilution of H_2 in CO_2; some of the H_2 was also converted to CO in the RWGS reaction, significantly affecting the OCP of the cell.

The non-linear decrease of OCP at ≥ 60 vol% CO_2 is explained by both the increased dilution of gases in CO_2 and the shifting equilibrium of the RWGS reaction. Fig. 1b shows the CO presence decreased significantly above 60 vol% CO_2, indicating a decreased presence of the RWGS reaction which, coupled with increased dilution of the gases in CO_2, caused the OCP to decrease non-linearly and to further deviate away from the Nernst potential under high CO_2 concentrations.

4.2 Utilisation of 50/50 vol% H_2/CO_2 mixtures

Fig. 2 shows the effect of decreasing the operating voltage on the products of the ESC when running on 50/50 vol% H_2/CO_2 in fuel cell mode. In agreement with Fig. 1, some of the initial H_2 and CO_2 were converted in the RWGS reaction to give an OCP of 0.92 V. As the cell voltage was progressively decreased, the electrical current produced increased, with a

maximum current of approx. 1235 mA cm^{-2} produced at 0.1 V. The H_2 and CO present were converted and the CO_2 increased.

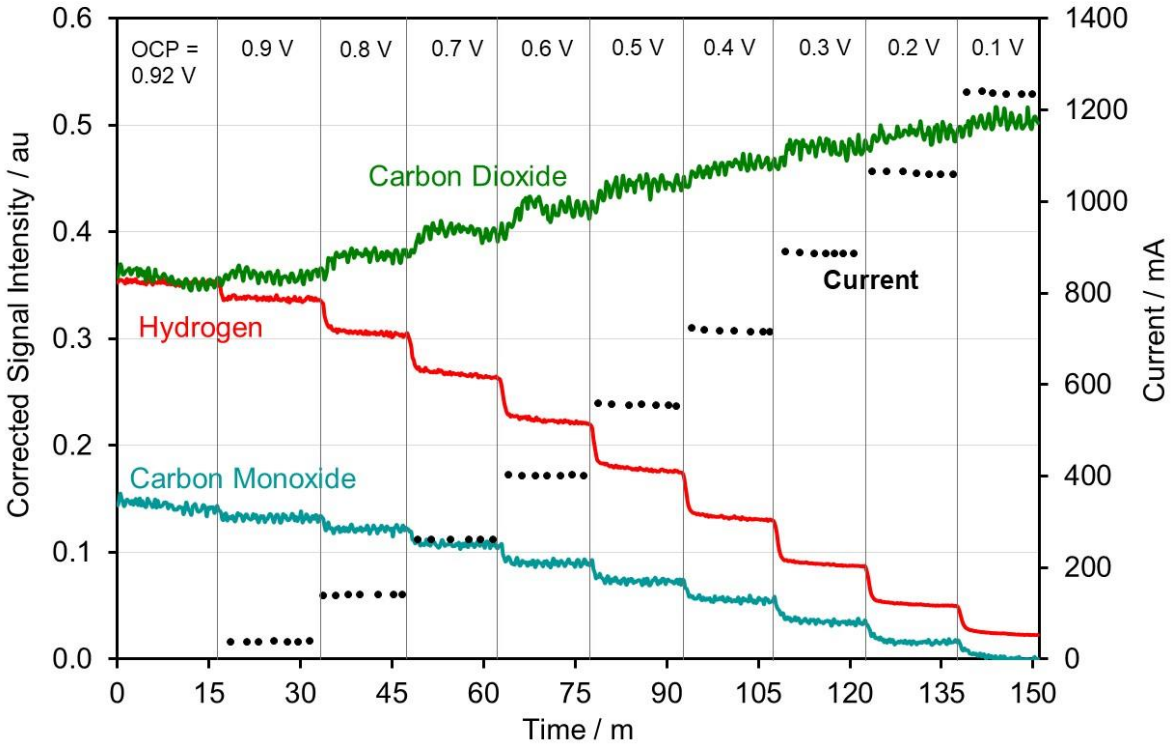

Fig. 2. The effect of operating voltage on the gaseous and current outputs of the ESC running on 50/50 vol% H_2/CO_2 in fuel cell mode at 800 °C. The figure plots the output gases on the primary vertical axis, and the corresponding current output on the secondary vertical axis.

It has previously been reported that provided the ratio of H_2 to CO is greater than 1, the electrochemical oxidation of H_2 on Ni-based SOC anodes is predominant and the rate of electrochemical CO oxidation is negligible [71-76]. Since the condition $H_2/CO > 1$ is satisfied across all the cell potentials studied in Fig. 2, the conversion of CO and subsequent CO_2 re-generation through the direct electrochemical oxidation of CO was not likely to be significant, and the current generated by the cell was produced predominantly from electrochemical oxidation of H_2.

The observed conversion of CO and subsequent regeneration of CO_2 was more likely due to a shift in equilibrium of the RWGS reaction imposed by electrochemical oxidation of H_2 (2),

which caused the partial pressure of H_2 to decrease and the partial pressure of H_2O to increase:

$$H_2 + O^{2-} \rightleftharpoons H_2O + 2e^- \quad (2)$$

As the potential of the cell was decreased therefore, the rate of electrochemical H_2 oxidation increased and the equilibrium of the RWGS reaction was shifted increasingly towards the Water-Gas Shift (WGS) reaction (3):

$$H_2O + CO \rightleftharpoons H_2 + CO_2 \quad (3)$$

The main pathway of CO_2 regeneration was therefore electrochemical oxidation of H_2 (2) followed by the WGS reaction (3).

Fig. 2 also illustrates that the electrical and gaseous products of SOFCs running on H_2/CO_2 mixtures varied significantly depending on the operating potential of the cell. The presence of CO in the output gases underlines the importance of ensuring high fuel utilisation efficiencies when running SOCs on H_2/CO_2 mixtures. Fig. 2 therefore indicates that due to the presence of the RWGS reaction, poor fuel utilisation efficiencies lead to emissions of CO.

Fig. 3 shows the effect of operating potential on the products of the ESC running on 50/50 vol% H_2/CO_2 in electrolysis mode. As the operating potential was increased, the partial pressure of CO_2 decreased, and the H_2 and CO increased. The synthesis gas production rate increased from approx. 12 $cm^3\ min^{-1}\ cm^{-2}$ at the OCP, to approx. 21 $cm^3\ min^{-1}\ cm^{-2}$ at 1.8 V. At the OCP, H_2-rich synthesis gas mixtures with a H_2/CO ratio of approximately 2.3 by volume were produced, whilst at the highest voltage studied (1.8 V) the H_2/CO ratio decreased to approx. 1.2 by volume. Fig. 3 suggests that with a fuel utilisation efficiency of 100%, a pure synthesis gas with a 1:1 H_2/CO ratio would be produced.

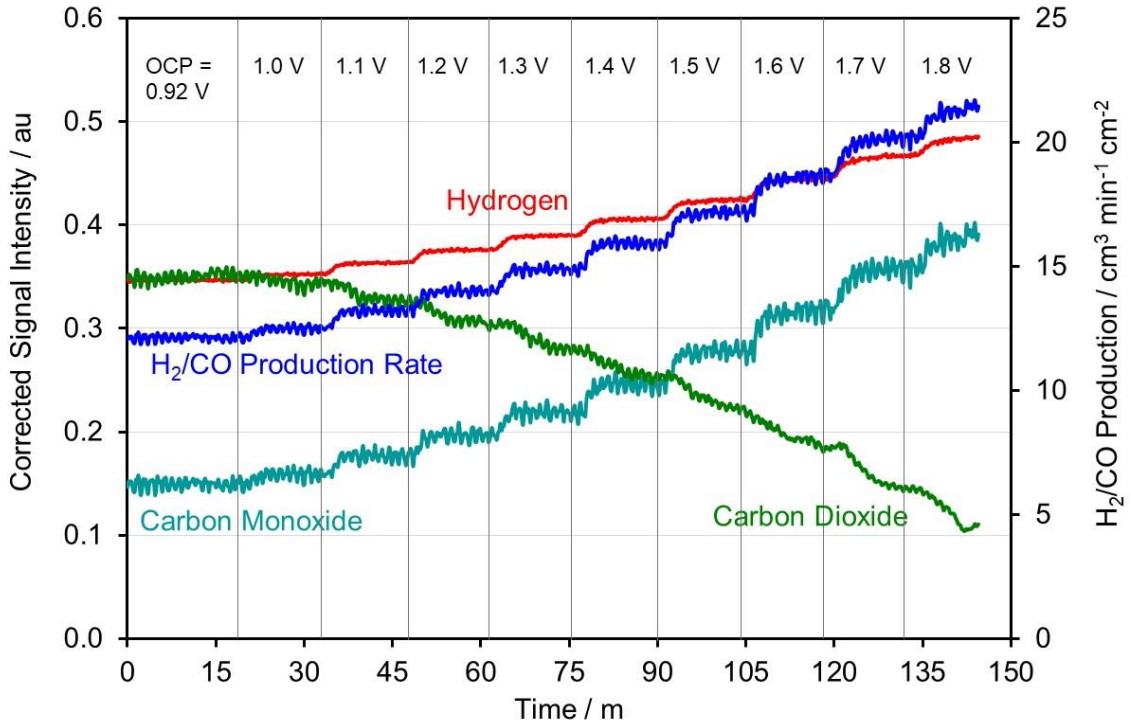

Fig. 3. The effect of operating voltage on the gaseous products of the ESC running on 50/50 vol% H_2/CO_2 in electrolysis mode at 800 °C. The figure plots the output gases from the anode on the primary vertical axis, and the corresponding total synthesis gas production (H_2 + CO) on the secondary vertical axis.

The regeneration of hydrogen was due to electrochemical reduction of H_2 (4) which is a relatively fast process:

$$H_2O + 2e^- \rightleftharpoons H_2 + O^{2-} \quad (4)$$

The observed decrease of the H_2/CO ratio indicates the rate of CO production increased relative to H_2 production as the operating voltage was increased. It is widely accepted that the rate of CO production through electrochemical CO_2 reduction (5) is slower than H_2 production through electrochemical H_2O reduction (4) [6-15, 71-76]:

$$CO_2 + 2e^- \rightleftharpoons CO + O^{2-} \quad (5)$$

Such a significant decrease of H_2/CO ratio is therefore unlikely to be explained by an increase in the rate of electrochemical CO_2 reduction alone. The presence of CO at the OCP indicates that CO production was also due to the RWGS reaction (1). It is likely therefore

that in electrolysis mode, the RWGS reaction was also promoted by electrochemical reduction of H_2O (4), which decreased the presence of H_2O and increased the H_2, shifting the equilibrium of the RWGS reaction (1) towards the production of CO. This is the reverse effect to that observed in fuel cell mode, where electrochemical oxidation of H_2 shifted the RWGS equilibrium towards the *conversion* of CO. Given that the presence of CO_2 was much greater than H_2O however, electrochemical reduction of CO_2 was also a probable pathway of CO production even though it is slower than H_2O reduction. With two simultaneously occurring CO production pathways, the rate of CO production increased relative to H_2 production as the operating voltage was decreased, therefore causing the H_2/CO ratio of the synthesis gas to decrease significantly.

4.3 Effects of fuel variability in fuel cell mode

The I-V and power curves in Fig. 4 show that the current and power produced in fuel cell mode were very sensitive to changes in the fuel composition, with significantly more current and power produced as the H_2 content of the fuel was increased. All I-V curves decreased non-linearly at high voltages, indicating the presence of activation losses. The I-V curves were almost parallel across the fuel composition range 100 - 40 vol% H_2, indicating similar activation losses for each fuel composition. Concentration losses were clearly observed for mixtures containing 20 vol% H_2 or less, where a non-linear decrease of voltage was observed below 0.5 V. However, the I-V curves clearly show that the efficiencies and electrical power output are not significantly affected by fuel variability provided the biohydrogen composition stays within the range 40-60 vol% H_2, particularly at high operating voltages.

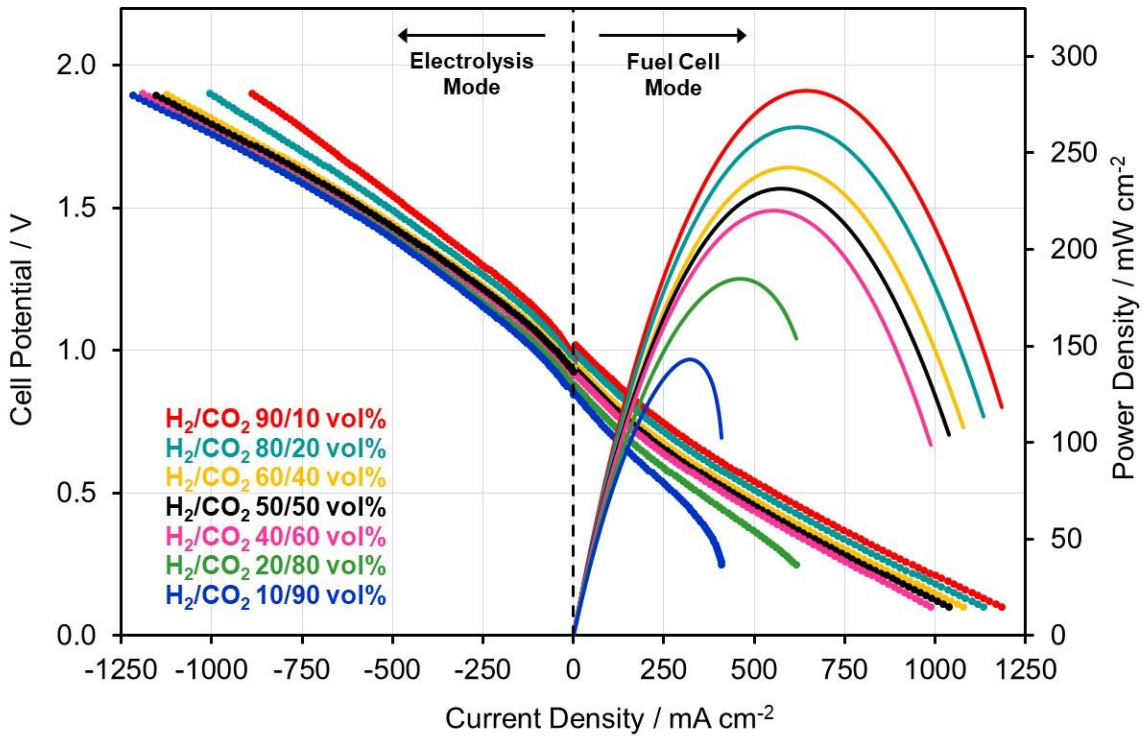

Fig. 4. The effect of H_2/CO_2 composition on the I-V curve of the ESC running in fuel cell mode and electrolysis mode at 800 °C. The corresponding fuel cell power curves are plotted on the secondary axis.

The electrochemical impedance spectra shown in Fig. 5, which were collected with the cell running on different H_2/CO_2 mixtures, were composed of two polarisation arcs. Zhan *et al*. have previously assigned the low frequency arc to gas diffusion losses and the high frequency arc to charge transfer and surface diffusion losses [77]. The widths of the arcs were measured and are shown in Table 3. In fuel cell mode, the width of the high frequency arc did not respond significantly to changes in the fuel composition across the entire fuel composition range studied, indicating that charge transfer and surface diffusion losses, whilst being relatively significant (approx. 0.52 Ω cm^2), were not sensitive to the composition of the fuel. This is also further evidence that electrical power production was through electrochemical oxidation of H_2 (2) only. Electrochemical oxidation of CO has previously been shown to cause a much higher activation overpotential compared with H_2 oxidation (2) [71-76]. Fig. 6 indicates that in fuel cell mode, the presence of CO varied significantly across different fuel mixtures due to the shifting equilibrium of the RWGS reaction. Therefore, if the

cell was utilising CO for power production, greater variation in the activation overpotential with fuel composition would be expected. The activation overpotentials were comparable across all compositions, indicating electrical current production by the cell was predominantly through the electrochemical oxidation of H_2.

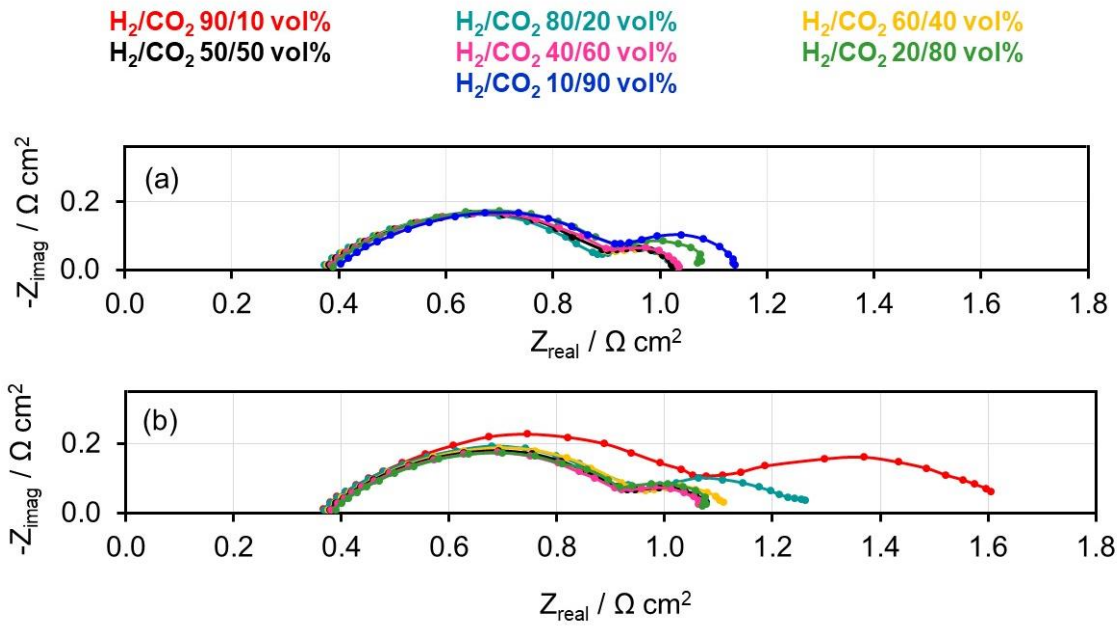

Fig. 5. The effect of H_2/CO_2 composition on the electrochemical impedance spectra of the ESC at 800 °C. Measurements were taken at: (a) OCP-0.1 V (fuel cell mode), and (b) OCP+0.1 V (electrolysis mode).

Table 3. Widths of the high and low frequency arcs in the electrochemical impedance spectra presented in Fig. 5.

	OCP-0.1 V (Fuel cell mode)		OCP+0.1 V (Electrolysis Mode)	
H_2/CO_2 vol%	High Frequency Arc Width / Ω cm^2	Low Frequency Arc Width / Ω cm^2	High Frequency Arc Width / Ω cm^2	Low Frequency Arc Width / Ω cm^2
90/10	0.5179	0.1316	0.7105	0.5290
80/20	0.5248	0.1245	0.5880	0.3039
60/40	0.5217	0.1214	0.5887	0.1444
50/50	0.5269	0.1240	0.5514	0.1460
40/60	0.5276	0.1530	0.5392	0.1415
20/80	0.5121	0.2255	0.5276	0.1530

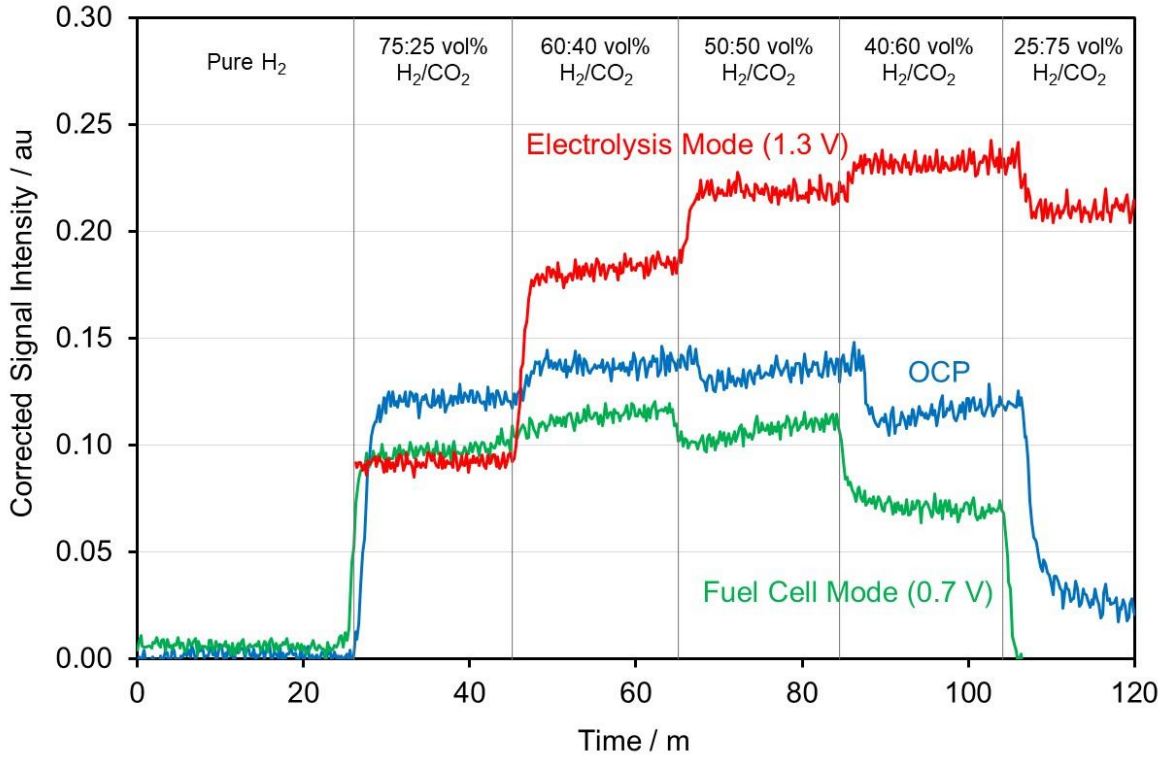

Fig. 6. Comparison of CO partial pressure in the anode output gases of the ESC when running on different fuel mixtures at 800 °C. Data are shown for the ESC when at OCP and when operating in fuel cell and electrolysis mode. The operating voltages are indicated on the figure.

The low frequency arc width also did not vary significantly in fuel cell mode for fuel mixtures in the range 50-90 vol% H_2, indicating that gas diffusion losses were not sensitive to the fuel composition in this range. For mixtures containing 50-90 vol% H_2 therefore, it was only the OCP losses that were sensitive to fuel variability as shown in Fig. 1. Decreasing the H_2 content from 50-20 vol% increased the low frequency arc width more significantly from 0.1240-0.2255 Ω cm^2 respectively, indicating that losses due to diffusion of H_2 through the anode were more important and sensitive to the fuel composition as the H_2 content was decreased below 50 vol%.

4.4 *Effects of fuel variability in electrolysis mode*

The I-V curves collected in electrolysis mode (see Fig. 4) show that activation losses were present in electrolysis mode, with a non-linear increase observed at 0.9 – 1.2 V that was more pronounced than the activation losses observed in fuel cell mode. In addition, there

was no non-linear behaviour observed at high voltages, indicating that unlike fuel cell mode, concentration losses were not observed to be significant in electrolysis mode. As was the case in fuel cell mode, the cell efficiency was not affected by fuel variability provided the biohydrogen composition stayed within the range 40-60 vol% H_2.

The electrochemical impedance spectra collected in electrolysis mode (see Fig. 5b) generally have wider polarisation arcs than those in fuel cell mode, indicating that the ESC operated less efficiently in electrolysis mode. Table 3 shows the high frequency arc widths were generally greater than in fuel cell mode, indicating increased charge transfer and surface diffusion losses. In addition, the width of the high frequency polarisation arc was sensitive to the fuel composition and decreased from 0.7105 - 0.5276 Ω cm^2 as the CO_2 content was increased. This contrasts with fuel cell mode, where activation overpotentials were not sensitive to fuel variability.

The low frequency polarisation arc widths were greater in electrolysis mode. CO_2 and H_2O are bigger in size than H_2 and CO and therefore caused greater gas diffusion overpotentials. The width of the low frequency arc and therefore the gas diffusion losses remained approximately constant across the range 40-80 vol% CO_2. When the CO_2 content was decreased below 40 vol% however, the arc width increased from 0.1444 - 0.5290 Ω cm^2, indicating that gas diffusion losses were very sensitive to fuel composition in this range.

Fig. 6 shows that CO production increased in electrolysis mode as the CO_2 content of the fuel was increased from 25 - 60 vol%. This was due to the activation and gas diffusion losses, which both decreased over this fuel range, as indicated by the decreasing widths of the high (activation) and low (diffusion) frequency arc widths of the impedance spectra (see Table 3). Fig. 6 shows the increase of CO production was particularly prevalent as the fuel mixture was changed from 75/25 - 60/40 vol% H_2/CO_2. The impedance data in Table 3 show the high frequency arc widths for 80/20 and 60/40 H_2/CO_2 mixtures were very similar (~ 0.588 Ω cm^2), whilst the low frequency arc width decreased significantly from 0.3039 Ω cm^2

to 0.1444 Ω cm^2. This indicates that the large increase of CO production observed from 75/25 - 60/40 vol% H_2/CO_2 was mainly due to improved diffusion efficiencies.

The behaviour of CO production in Fig. 6 and the impedance data in Table 3 are also further evidence that CO production occurred simultaneously through the RWGS reaction and electrochemical reduction of CO_2. Table 3 indicates that the activation and gas diffusion potentials continued to decrease (the arc widths decrease) as the CO_2 content was increased to 80 vol%, suggesting that CO production should also have continued to increase as the CO_2 content was increased. Fig. 6 shows this was not the case above 60 vol% CO_2 where a clear decrease in CO production was observed. The CO production at OCP (which was entirely due to the RWGS reaction) decreased when the CO_2 content was greater than 60 vol% due to a shift in the equilibrium of the RWGS reaction. The observed decrease of CO above 60 vol% CO_2 in electrolysis mode therefore indicates that CO production could not entirely have been due to electrochemical reduction of CO_2, and that the RWGS reaction was also a significant reaction pathway of CO production.

Fig. 7 shows the variation in the quantity and composition of the synthesis gas produced as the fuel composition was changed. It is clear that fuel variability significantly influenced the composition and quantity of syngas produced by the cell in electrolysis mode. Increasing the CO_2 content from 25 - 75 vol% decreased the total production of synthesis gas from 20 - 9 $cm^3\ min^{-1}\ cm^{-2}$. The H_2/CO ratio of the synthesis gas also decreased significantly from approximately 7.9 - 0.7 by volume, although the variation was less over the range 40 - 60 vol% CO_2. The sharp decrease of H_2/CO ratio observed as the fuel mixture was changed from 25 - 40 vol% CO_2 was due to the decrease of CO_2 gas diffusion overpotential (see Table 3) as described earlier. The H_2/CO ratio continued to decrease from 40-60 vol% CO_2 due to a mixture of increased CO production and direct displacement of H_2 with CO_2 in the initial fuel mixture. Despite a loss of CO production above 60 vol% CO_2 (see Fig. 6), the H_2/CO ratio again decreased due to direct displacement of H_2 with CO_2.

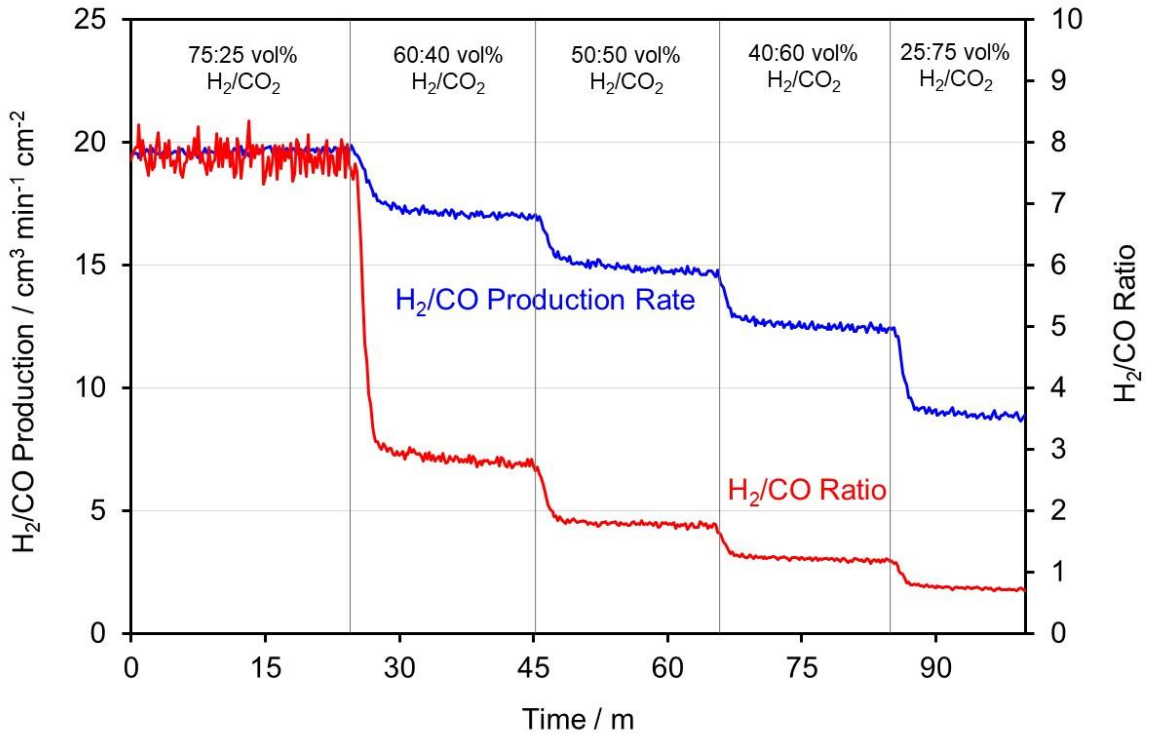

Fig. 7. The effect of H_2/CO_2 composition on the products of the ESC running in electrolysis mode at 800 °C. The operating voltage of the cell was 1.3 V. The figure shows the synthesis gas production (H_2 + CO) on the primary vertical axis and the composition of the synthesis gas (H_2/CO ratio) on the secondary vertical axis.

Since synthesis gas is composed of CO and H_2, the decrease of H_2/CO production rate as the CO_2 content was increased was partly due to direct displacement of H_2 with CO_2 in the initial fuel mixture. Even though the CO production increased as the CO_2 content was increased up to 60 vol% (see Fig. 6) therefore, CO was not produced at a fast enough rate to give an overall increase of H_2/CO production rate. The drop in H_2/CO production was more pronounced as the CO_2 content was increased from 60 – 75 vol%, which was likely due to the loss of CO produced from the RWGS reaction (see Fig. 6) as described earlier. Therefore, even though the OCP and the activation and gas diffusion overpotentials were improved as the CO_2 partial pressure was increased, the displacement of H_2 with CO_2 in the initial fuel mixture and the loss of the RWGS reaction caused the overall synthesis gas production rate to decrease, highlighting the importance of the RWGS reaction in the production of CO.

5. Conclusions

Fuel variability is an issue that is applicable to the utilisation of many gaseous renewable and waste feedstocks in SOC devices. In this work, the utilisation of H_2/CO_2 mixtures in SOCs was investigated experimentally using a combination of electrochemical techniques and quadrupole mass spectrometry, showing SOC performance and fuel processing in greater detail than has been achieved previously. In addition, solid oxide electrolysis of biohydrogen has been investigated for the first time and was compared directly with fuel cell mode utilisation. The main conclusions are:

- The performance, fuel processing, electrical power production and output gas composition of SOC devices running on H_2/CO_2 mixtures are very sensitive to variation in the inlet feedstock composition, demonstrating the need for SOC anode materials and designs that minimise the effects of fuel variability on SOC performance and stability.
- However, the cell performance is not significantly affected by fuel variability when the biohydrogen composition stays within the range 40-60 vol% H_2.
- Solid oxide electrolysis of H_2/CO_2 mixtures to yield synthesis gas was demonstrated, illustrating the increased versatility of biohydrogen (H_2/CO_2) compared with methane-based biogas (CH_4/CO_2) mixtures. Syngas production rates and composition are dependent on the initial fuel composition and cell operating voltage.
- H_2O and CO production takes place *in-situ* on the anode via the reverse water-gas shift (RWGS) reaction and had a significant effect on the mechanism of reactant conversion and the OCP of the cell.
- In fuel cell mode, electrical power is produced predominantly via the electrochemical oxidation of H_2. CO does not contribute to power production and is instead converted via the WGS reaction to regenerate CO_2.
- In electrolysis mode, CO production takes place through electrochemical CO_2 reduction and the RWGS reaction simultaneously. H_2 is regenerated through electrochemical reduction of H_2O.

- Increasing the H_2 content of the inlet fuel composition generally decreases the overpotentials when running in fuel cell mode, giving increased power production. The electrical power output of the cell is not significantly affected by fuel variability provided the biohydrogen composition stays within the range 40-60 vol% H_2.
- In electrolysis mode, overpotentials are decreased by increasing the CO_2 of the fuel; however, this does not necessarily yield increased synthesis gas production rates or a consistent H_2/CO ratio, since CO is produced through the RWGS reaction as well as electrochemical CO_2 reduction.

Acknowledgements

The authors would like to acknowledge the funding provided for this work through the FLEXIS project (C80835). FLEXIS is part-funded by the European Regional Development Fund (ERDF), through the Welsh Government.

References

[1] Steele BCH. Material science and engineering: the enabling technology for the commercialisation of fuel cell systems. J Mater Sci 2001;36:1053-68.

[2] Ormerod RM. Solid oxide fuel cells. Chem Soc Rev 2003;32:17-28.

[3] Stambouli AB, Traversa E. Solid oxide fuel cells (SOFCs): a review of an environmentally clean and efficient source of energy. Renew Sustainable Energy Rev 2002;6:433-55.

[4] Singhal SC. Advances in solid oxide fuel cell technology. Solid State Ion 2002;135:305-13.

[5] Yamamoto O. Solid oxide fuel cells: fundamental aspects and prospects. Electrochim Acta 2000;45:2423-35.

[6] Ni M, Leung MKH, Leung DYC. Technological development of hydrogen production by solid oxide electrolyzer cell (SOEC). Int J Hydrogen Energy 2008;33:2337-54.

[7] Laguna-Bercero MA. Recent advances in high temperature electrolysis using solid oxide fuel cells: a review. J Power Sources 2012;203:4-16.

[8] Brisse A, Schefold J, Zahid M. High temperature water electrolysis in solid oxide cells. Int J Hydrogen Energy 2008;33:5375-82.

[9] Ebbesen SD, Mogensen M. Electrolysis of carbon dioxide in solid oxide electrolysis cells. J Power Sources 2009;193:349-58.

[10] Hauch A, Ebbesen SD, Jensen SH, Mogensen M. Highly efficient high temperature electrolysis. J Mater Chem 2008;18:2331-40.

[11] Graves C, Ebbesen SD, Mogensen M. Co-electrolysis of CO_2 and H_2O in solid oxide cells: performance and durability. Solid State Ion 2011;192:398-403.

[12] Zheng Y, Wang JC, Yu B, Zhang WQ, Chen J, Qiao JL, Zhang JJ. A review of high temperature co-electrolysis of H_2O and CO_2 to produce sustainable fuels using solid oxide electrolysis cells (SOECs): advanced materials and technology. Chem Soc Rev 2017;46:1427-63.

[13] Kazempoor P, Braun RJ. Hydrogen and synthetic fuel production using high temperature solid oxide electrolysis cells (SOECs). Int J Hydrogen Energy 2015;40:3599-612.

[14] Gómez SY, Hotza D. Current developments in reversible solid oxide fuel cells. Renew Sustainable Energy Rev 2016;61:155-74.

[15] Ferrero D, Lanzini A, Santarelli A, Leone P. A comparative assessment on hydrogen production from low- and high-temperature electrolysis. Int J Hydrogen Energy 2013;38:3523-36.

[16] Galvagno A, Chiodo V, Urbani F, Freni F. Biogas as hydrogen source for fuel cell applications. Int J Hydrogen Energy 2013;38:3913-20.

[17] Shiratori Y, Ijichi T, Oshima T, Sasaki K. Internal reforming SOFC running on biogas. Int J Hydrogen Energy 2010;35:7905-12.

[18] Staniforth J, Kendall K. Biogas powering a small tubular solid oxide fuel cell. J Power Sources 1998;71:275-77.

[19] Staniforth J, Ormerod RM. Implications for using biogas as a fuel source for solid oxide fuel cells: internal dry reforming in a small tubular solid oxide fuel cell. Catal Lett 2002;81:19-23.

[20] Staniforth J, Ormerod RM. Running solid oxide fuel cells on biogas. Ionics 2003;9:336-41.

[21] Ma JJ, Jiang CR, Connor PA, Cassidy M, Irvine JTS. Highly efficient, coking-resistant SOFCs for energy conversion using biogas fuels. J Mater Chem 2015;3:19068-76.

[22] van Herle J, Schuler A, Dammann L, Bosco M, Truong TB, de Boni E, Hajbolouri F, Vogel F, Scherer GG. Fuels for fuel cells: requirements and fuel processing. Chimia 2004;58:887-95.

[23] Prodromidis GN, Coutelieris FA. Thermodynamic analysis of biogas fed solid oxide fuel cell power plants. Renew Energy 2017;108:1-10.

[24] Leone P, Lanzini A, Santarelli M, Cali M, Sagnelli F, Boulanger A, Scaletta A, Zitella P. Methane-free biogas for direct feeding of solid oxide fuel cells. J Power Sources 2010;195:239-248.

[25] Leone P, Lanzini A, Santarelli A, Zitella P, Quaglia MC. Feasibility of SOFC operation with bio-methane and bio-hydrogen from anaerobic digestion. ECS Trans 2009;17:185-95.

[26] Razbani O, Assadi M, Andersson M. Three dimensional CFD modeling and experimental validation of an electrolyte supported solid oxide fuel cell fed with methane-free biogas. Int J Hydrogen Energy 2013;38:10068-80.

[27] Paradis H, Andersson A, Yuan J, Sundén B. Simulation of alternative fuels for potential utilization in solid oxide fuel cells. Int J Energy Res 2011;35:1107-17.

[28] Razbani O, Assadi M. Performance of a biohydrogen solid oxide fuel cell. Int J Hydrogen Energy 2013;38:13781-91.

[29] La Licata B, Sagnelli F, Boulanger A, Lanzini A, Leone P, Zitella P, Santarelli M. Bio-hydrogen production from organic wastes in a pilot plant reactor and its use in a SOFC. Int J Hydrogen Energy 2011;36:7861-65.

[30] Lebreton M, Delanoue B, Baron E, Ricoul F, Kerihuel A, Subrenat A, Joubert O, Le Gal Le Salle A. Effects of carbon monoxide, carbon dioxide, and methane on nickel/yttria-stabilised zirconia-based solid oxide fuel cells performance for direct coupling with gasifier. Int J Hydrogen Energy 2015;40:10231-41.

[31] Ricoul F, Subrenat A, Joubert O, Le Gal Le Salle A. Electricity production from lignocellulosic biomass by direct coupling of a gasifier and a Nickel/Yttria-stabilized Zirconia-based solid oxide fuel cell. Part 1: From gas production to direct electricity production. Int J Hydrogen Energy 2017;42:21215-25.

[32] Ozcan H, Dincer I. Performance evaluation of an SOFC based trigeneration system using various gaseous fuels from biomass gasification. Int J Hydrogen Energy 2015;40:7798-807.

[33] Le Gal Le Salle A, Ricoul F, Joubert O, Kerihuel A, Subrenat A. Electrochemical study of a SOFC with various H_2-CO-CH_4-CO_2-N_2 gaseous mixtures. Fuel Cells 2017;17:144-50.

[34] Monaco F, Lanzini A, Santarelli M. Making synthetic fuels for the road transportation sector via solid oxide electrolysis and catalytic upgrade using recovered carbon dioxide and residual biomass. J Clean Prod 2018;170:160-73.

[35] Hansen JB, Christiansen N, Nielsen JU. Production of Sustainable Fuels by Means of Solid Oxide Electrolysis. ECS Trans 2011;35:2941-48.

[36] Pati S, Gopalan S, Pal UB. A solid oxide membrane electrolyzer for production of hydrogen and syn-gas from steam and hydrocarbon waste in a single step. Int J Hydrogen Energy 2011;36:152-9.

[37] Ramirez-Minguela JJ, Rangel-Hernandez VH, Alfaro-Ayala JA, Uribe-Ramirez AR, Mendoza-Miranda JM, Belman-Flores JM, Ruiz-Camacho B. Energy and entropy study of a SOFC using biogas from different sources considering internal reforming of methane. Int J Heat Mass Transfer 2018;120:1044-54.

[38] Rasi S, Veijanen A, Rintala J. Trace compounds of biogas from different biogas production plants. Energy 2007;32:1375-80.

[39] Ryckebosch E, Drouillon M, Veruaeren H. Techniques for transformation of biogas to biomethane. Biomass Bioenergy 2011;35:1633-45.

[40] Papurello D, Iafrate C, Lanzini A, Santarelli M. Trace compounds impact on SOFC performance: Experimental and modelling approach. Appl Energy 2017;208:637-654.

[41] Elizalde-Blancas F, Celik IB, Rangel-Hernandez V, Hernandez-Guerrero A, Riesco-Avila JM. Numerical modeling of SOFCs operating on biogas from biodigesters. Int J Hydrogen Energy 2013;38:377-84.

[42] Baron S, Brandon N, Atkinson A, Steele B, Rudkin R. The impact of wood-derived gasification gases on Ni-CGO anodes in intermediate temperature solid oxide fuel cells. J Power Sources 2004;126:58-66.

[43] Balat M, Balat M, Kırtay E, Balat H. Main routes for the thermo-conversion of biomass into fuels and chemicals. Part 2: Gasification systems. Energy Convers Manag 2009;50:3158-68.

[44] Uribe-Soto W, Portha JF, Commenge JM, Falk L. A review of thermochemical processes and technologies to use steelworks off-gases. Renew Sustainable Energy Rev 2017;74:809-23.

[45] Murgi N, De Lorenzo G, Corigliano O, Mirandola FA, Fragiacomo P. Influence of Anodic Gas Mixture Composition on Solid Oxide Fuel Cell Performance: Part 2. Int J Heat Technol 2016;34:S309-14.

[46] Baldinelli A, Barelli L, Bidini G. Performance characterization and modelling of syngas-fed SOFCs (solid oxide fuel cells) varying fuel composition. Energy 2015;90:2070-84.

[47] Borello D, Di Carlo A, Boigues-Munoz C, McPhail SJ, Cinti G, Penchini D. The Influence of Bio-syngas Composition on the Derating of Solid Oxide Fuel Cells. Energy Procedia 2014;61:1099-102.

[48] Andersson M, Paradis H, Yuan J, Sundén B. Modeling analysis of different renewable fuels in an anode supported SOFC. J Fuel Cell Sci Technol 2011;8:031013.

[49] Laycock CJ, Staniforth JZ, Ormerod RM. Biogas as a fuel for solid oxide fuel cells and synthesis gas production: effects of ceria-doping and hydrogen sulfide on the performance of nickel-based anode materials. Dalton Trans 2011;40:5494-504.

[50] Sasaki K, Haga K, Yoshizumi T, Minematsu D, Yuki E, Liu RR, Uryu C, Oshima T, Ogura T, Shiratori Y, Ito K, Koyama M, Yokomoto K. Chemical durability of solid oxide fuel cells: influence of impurities on long-term performance. J Power Sources 2011;196:9130-40.

[51] Haga K, Adachi S, Shiratori Y, Itoh K, Sasaki K. Poisoning of SOFC anodes by various fuel impurities. Solid State Ion 2008;179:1427-31.

[52] Rasmussen JFB, Hagen A. The effect of H_2S on the performance of Ni-YSZ anodes in solid oxide fuel cells. J Power Sources 2009;191:534-41.

[53] Madi H, Diethelm S, Ludwig C, Van Herle J. Organic-sulfur poisoning of solid oxide fuel cell operated on bio-syngas. Int J Hydrogen Energy 2016;41:12231-41.

[54] Park SD, Vohs JM, Gorte RJ. Direct oxidation of hydrocarbons in a solid-oxide fuel cell. Nature 2000;404:265-7.

[55] Guwy AJ, Dinsdale RM, Kim JR, Massanet-Nicolau J, Premier G. Fermentative biohydrogen production systems integration. Bioresour Technol 2011;102:8534-42.

[56] Manish S, Banerjee R. Comparison of biohydrogen production processes. Int J Hydrogen Energy 2008;33:279-86.

[57] Kalinci Y, Hepbasli A, Dincer I. Biomass-based hydrogen production: A review and analysis. Int J Hydrogen Energy 2009;34:8799-817.

[58] Cavinato C, Bolzonella D, Fantone F, Cecchi F, Pavan P. Optimization of two-phase thermophilic anaerobic digestion of biowaste for hydrogen and methane production through reject water recirculation. Bioresour Technol 2011;102:8605-11.

[59] Peila P, Tokarz W, Kazmierczak W, Detman A, Sikora A, Piotrowski J. The use of hydrogen-rich gas obtained from dark fermentation of molasses from sugar industry for fueling a fuel cell. Przemysl Chemiczny 2016;95:993-99.

[60] Patterson T, Esteves S, Dinsdale R, Guwy A, Maddy J. Life cycle assessment of biohydrogen and biomethane production and utilisation as a vehicle fuel. Bioresour Technol 2013;131:235-45.

[61] Bharathiraja B, Sudharsanaa T, Bharghavi A, Jayamuthunagai J, Praveenkumar R. Biohydrogen and Biogas - An overview on feedstocks and enhancement process. Fuel 2016;185:810-28.

[62] Angelidaki I, Treu L, Tsapekos P, Luo G, Campanaro S, Wenzel H, Kougias PG. Biogas upgrading and utilization: current status and perspectives. Biotechnol Adv 2018;in press.

[63] Mohamad IN, Rohani R, Nor MTM, Claassen P, Abd Rahaman MS, Masdar MSM, Rosli MI. An overview of gas upgrading technologies for biohydrogen produced from treatment of palm oil mill effluent. J Eng Sci Technol 2017;12:725-55.

[64] Khan IU, Othman MHD, Hashim H, Matsuura T, Ismail AF, Arzhandi MRD, Azelee IW. Biogas as a renewable energy fuel - A review of biogas upgrading, utilisation and storage. Energy Convers Manag 2017;150:277-94.

[65] Da Silva AL, Heck NC. Oxide incorporation into Ni-based solid oxide fuel cell anodes for enhanced sulfur tolerance during operation on hydrogen or biogas fuels: A comprehensive thermodynamic study. Int J Hydrogen Energy 2015;40:2334-53.

[66] Wolf A, Jess A, Kern C. Syngas production via reverse water-gas shift reaction over a Ni-Al_2O_3 catalyst: catalyst stability, reaction kinetics, and modelling. Chem Eng Technol 2016;39:1040-48.

[67] Wang L, Liu H, Liu Y, Chen Y, Yang S. Influence of preparation method on performance of Ni-CeO_2 catalysts for reverse water-gas shift reaction. J Rare Earths 2013;31:559-64.

[68] Lim JY, McGregor J, Sederman AJ, Dennis JS. The role of the boudouard and water-gas shift reactions in the methanation of CO or CO_2 over Ni/γ-Al_2O_3 catalyst. Chem Eng Sci 2016;152:754-66.

[69] Lu B, Kawamoto K. Preparation of mesoporous CeO_2 and monodispersed NiO particles in CeO_2, and enhanced selectivity of NiO/CeO_2 for reverse water gas shift reaction. Mater Res Bull 2014;53:70-8.

[70] Fiaxell SOFC Technologies. http://www.fiaxell.com; 2015 [accessed 04.08.17].

[71] Holtappels P, De Haart LGJ, Stimming U, Vinke IC, Mogensen M. Reaction of CO/CO_2 gas mixtures on Ni–YSZ cermet electrodes. J Appl Electrochem 1999;29:561-68.

[72] Matsuzaki Y, Yasuda I. Electrochemical oxidation of H_2 and CO in a $H_2 – H_2O – CO – CO_2$ system at the interface of a Ni-YSZ cermet electrode and YSZ electrolyte. J Electrochem Soc 2000;147:1630-35.

[73] Weber A, Sauer B, Müller AC, Herbstritt D, Tiffée EI. Oxidation of H_2, CO and methane in SOFCs with Ni/YSZ-cermet anodes. Solid State Ion 2002;152-153:543-50.

[74] Jiang Y, Virkar AV. Fuel Composition and Diluent Effect on Gas Transport and Performance of Anode-Supported SOFCs. J Electrochem Soc 2003;150:A942-51.

[75] Andersson A, Yuan J, Sundén B. SOFC modeling considering hydrogen and carbon monoxide as electrochemical reactants. J Power Sources 2013;232:42-54.

[76] Kulkarni K, Giddey S, Badwal SPS. Efficient conversion of CO2 in solid oxide electrolytic cells with Pd doped perovskite cathode on ceria nanofilm interlayer. J CO2 Utilization 2017;17:180-7.

[77] Zhan Z, Kobsiriphat W, Wilson JR, Pillai M, Kim I, Barnett SA. Syngas production by coelectrolysis of CO_2/H_2O: the basis for a renewable energy cycle. Energy Fuels 2009;23:3089-96.